Earth and Planetary Science Letters 621 (2023) 118373

Contents lists available at ScienceDirect

Earth and Planetary Science Letters

journal homepage: www.elsevier.com/locate/epsl

Synchronising rock clocks of Mars' history: Resolving the shergottite $^{40}Ar/^{39}Ar$ age paradox

Benjamin E. Cohen [a,b,c,*], Darren F. Mark [a,d], William S. Cassata [e], Lara M. Kalnins [c], Martin R. Lee [b], Caroline L. Smith [b,f], David L. Shuster [g,h]

[a] Scottish Universities Environmental Research Centre (SUERC), East Kilbride, UK
[b] School of Geographical and Earth Sciences, University of Glasgow, UK
[c] School of GeoSciences, University of Edinburgh, UK
[d] Department of Earth and Environmental Sciences, University of St Andrews, UK
[e] Lawrence Livermore National Laboratory, CA, USA
[f] Department of Earth Sciences, The Natural History Museum, London, UK
[g] Department of Earth and Planetary Science, University of California, Berkeley, CA, USA
[h] Berkeley Geochronology Center, Berkeley, CA, USA

ARTICLE INFO

Article history:
Received 12 June 2023
Received in revised form 29 August 2023
Accepted 31 August 2023
Available online 15 September 2023
Editor: F. Moynier

Keywords:
shergottite
Mars
$^{40}Ar/^{39}Ar$ geochronology

ABSTRACT

The shergottites are the most abundant and diverse group of Martian meteorites and provide unique insights into the mafic volcanic and igneous history of Mars. Their ages, however, remain a source of debate. Different radioisotopic chronometers, including $^{40}Ar/^{39}Ar$, have yielded discordant ages, leading to conflicting interpretations on whether the shergottites originate from young (mostly <700 Ma) or ancient (>4,000 Ma) Martian volcanoes. To address this issue, we have undertaken an $^{40}Ar/^{39}Ar$ investigation of seven shergottite meteorites utilizing an innovative approach to correcting data for cosmogenic isotope production and resolution of initial trapped components which, crucially, do not require assumptions concerning the sample's geologic context. Our data yield statistically robust $^{40}Ar/^{39}Ar$ isochron ages ranging from 161 ± 9 Ma to 540 ± 63 Ma (2σ), synchronous with the U-Pb, Rb-Sr, and Sm-Nd ages for the respective meteorites. These data indicate that, despite experiencing shock metamorphism, the shergottites were sourced from the youngest volcanoes on Mars.

1. Introduction

The Perseverance rover is currently exploring the geologic history of Jezero Crater on Mars including its past habitability. The mission is also caching high-priority samples to return for in-depth analysis in terrestrial laboratories (Farley et al., 2022). Sample return, however, remains a tantalizing future prospect, and there is much that can be learned about the red planet from the more than 350 Martian meteorites already in terrestrial collections (Meteoritical Bulletin Database). The largest and most diverse group of Martian meteorites are the shergottites (n > 290 specimens), which represent over 80% of the available samples from Mars (Meteoritical Bulletin Database). They were sourced from volcanic and intrusive igneous rocks close to the surface of Mars, and ejected from the planet's surface via a series of temporally distinct large impact events at multiple locations, before being captured by Earth's gravity and falling as meteorites (Nyquist et al., 2001; Herzog and Caffee, 2014; McSween and McLennan, 2014).

One of the most important constraints for Martian meteorites are their age; as they are obviously not collected *in situ*, accurate and precise ages provide critical information about their potential source locations on Mars, via linking the meteorite data (i.e., age, chemistry, rock type) with geological maps and other remotely sensed data of the Martian surface. However, the $^{40}Ar/^{39}Ar$ chronometer has frequently yielded varying ages for the shergottites (Fig. 1A, Table S1). For example, the meteorite Zagami has reported $^{40}Ar/^{39}Ar$ ages ranging from 198 Ma to nearly 2000 Ma, while other shergottites have results up to 3000 Ma (Bogard and Garrison, 1999; Bogard and Park, 2008; Korochantseva et al., 2009; Park et al., 2013b). The $^{40}Ar/^{39}Ar$ data are also often internally discordant (i.e., different ages for the same meteorite) and, unusually, much older than the ages derived from other isotopic systems (Fig. 1A, Table S1). Other radioisotopic chronometers (U-Pb, Sm-Nd, Lu-Hf, Rb-Sr) when applied to the shergottites yield ages as young as ca. 160 Ma, which would imply that their volcanic sources are

* Corresponding author at: Scottish Universities Environmental Research Centre (SUERC), East Kilbride, UK.
E-mail address: ben.cohen@glasgow.ac.uk (B.E. Cohen).

https://doi.org/10.1016/j.epsl.2023.118373

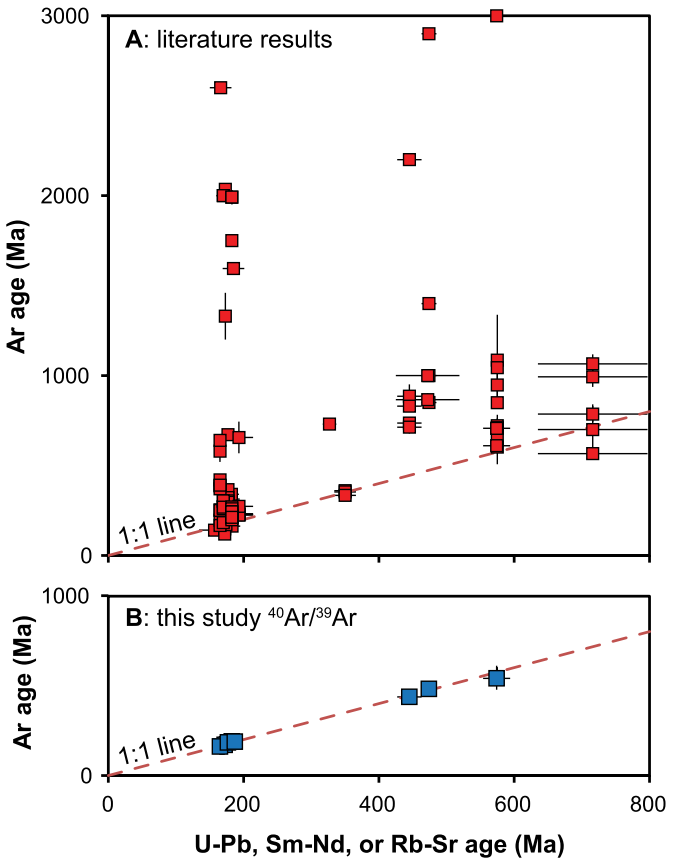

Fig. 1. Comparison of published $^{40}Ar/^{39}Ar$ results vs. this study. (A) The majority of published $^{40}Ar/^{39}Ar$ results for the shergottite meteorites greatly exceed the ages determined from other chronometers, leading to interpretations that the ages were affected by excess or parentless argon (Bogard and Garrison, 1999; Bogard et al., 2009; Korochantseva et al., 2009; Park et al., 2013a,b) or variable resetting of geochronometers by shock metamorphism (Bouvier et al., 2005, 2008). Data sources for these ages are listed in Table S1. **(B)** In contrast, $^{40}Ar/^{39}Ar$ ages from this study (blue squares) are concordant with other chronometers applied to these meteorites. Analytical uncertainties are smaller than the symbols or indicated by error bars (2σ).

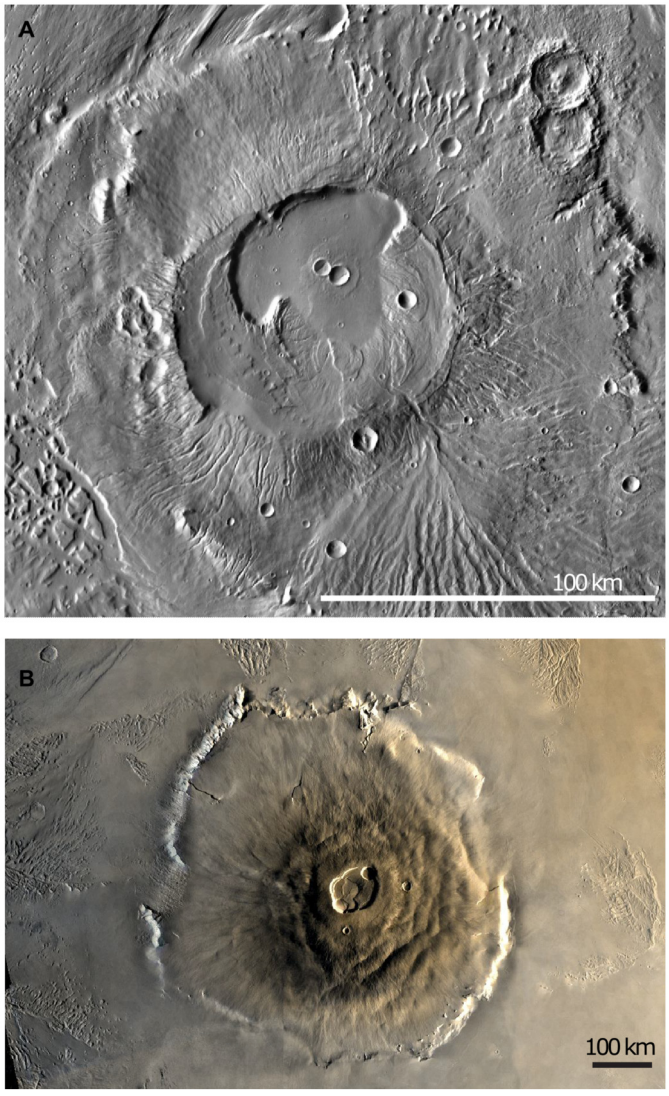

Fig. 2. Are shergottites from ancient or youthful Mars? (A) Old ages for the shergottites indicate derivation from ancient and heavily cratered volcanic units, often affected by surface water, e.g., Apollinaris Mons, a moderate sized (~ 280 × 190 km) eroded edifice with an age of 3600-3800 Ma (Werner, 2009), and situated ~160 km north of Gusev Crater, the site of the Martian Exploration Rover Spirit. Daytime-IR THEMIS mosaic (Christensen et al., 2004). **(B)** Conversely, ages of predominately <700 Ma demonstrate that the shergottites are derived from eruptions of the youngest and largest volcanoes on Mars, like the 840 × 640 km Olympus Mons (Image: NASA/NSSDCA).

amongst the youngest features on Mars (McSween and McLennan, 2014; Herd et al., 2017; Lapen et al., 2017).

Geochronological interpretations of the shergottites are complicated further as these meteorites experienced impact-generated shock metamorphism, producing pressures of 16 to <50 GPa and temperatures ranging from 70 °C to more than 1000 °C above ambient. The exact P-T conditions differ greatly between meteorites, and even within the same meteorite (Fritz et al., 2005, 2017; Hu et al., 2023) (Table 1). As the $^{40}Ar/^{39}Ar$ system has relatively low closure temperatures (typically between 200 to 400 °C, depending on mineralogy), and can be susceptible to Ar loss, it is even more unusual that the $^{40}Ar/^{39}Ar$ ages are at face value older – rather than younger – than chronometers with high closure temperatures (e.g., U-Pb). It has been suggested by some authors that all shergottite age data (U-Pb, Sm-Nd, Lu-Hf, Rb-Sr, as well as $^{40}Ar/^{39}Ar$) are either partially or fully reset and do not record a primary igneous crystallization event, with the exception of the Pb-Pb model ages of >4000 Ma (e.g., Bouvier et al., 2005, 2008; El Goresy et al., 2013).

Nevertheless, shock metamorphism is a highly heterogeneous process, and many meteorites and portions within them did not experience high P-T conditions (Fritz et al., 2005, 2017; Hu et al., 2023). Several recent studies have demonstrated that the U-Pb, Sm-Nd, Lu-Hf, and Rb-Sr chronometers do record concordant and consistent ages from the least-shocked portions of the shergottites, with these results interpreted as igneous crystallization ages (e.g., McSween and McLennan, 2014; Herd et al., 2017; Lapen et al., 2017; Staddon et al., 2021; McFarlane and Spray, 2022). The >4000 Ma Pb-Pb model ages are interpreted to reflect either ancient Martian differentiation events and/or meteorite contamination with Martian or terrestrial Pb (Jones, 2015; Bellucci et al., 2016; Borg et al., 2016).

These two contrasting interpretations of geochronologic data have profound implications for our understanding of the evolution of Mars. If the shergottites are >4000 Ma (e.g., Bouvier et al., 2005, 2008; El Goresy et al., 2013), then they must be derived from ancient Martian terrains that are heavily cratered (Tanaka et al., 2014) (Fig. 2A) and indicate early segregation of chemical reservoirs in the Martian mantle. Conversely, young ages suggest the shergottites sample large shield edifices, such as Olympus Mons (Tanaka et al., 2014) (Fig. 2B) and demonstrate that geochemical reservoirs on Mars have remained unmixed for most of its history.

To address these issues, we have undertaken an $^{40}Ar/^{39}Ar$ investigation of seven shergottite meteorites. We have used a novel approach to treatment of extra-terrestrial $^{40}Ar/^{39}Ar$ data (Cassata and Borg, 2016), which has a more accurate methodology to determine the contributions from cosmogenic Ar. We have also used isotope correlation plots for data interpretation, as they do not require assumptions regarding the value of the trapped $^{40}Ar/^{36}Ar$ component within each analysis (i.e., if the sample contains trapped Martian atmosphere, trapped terrestrial atmosphere, or some mixture of the two). We find that our $^{40}Ar/^{39}Ar$ ages are synchronous with those determined using the U-Pb, Sm-Nd, Lu-Hf, and Rb-Sr dating techniques. Our data also suggest that despite experiencing shock metamorphism, the intensity and duration of shock was sufficiently heterogeneous and short that the Ar systematics of the shergottite minerals were largely unchanged and retained their magmatic cooling ages rather than being reset, supporting the interpretation that the shergottite meteorites are indeed from the youngest volcanoes on Mars.

2. Materials and methods

We have analyzed seven shergottites: Alan Hills (ALH) 77005, Dar al Gani (DaG) 476, Los Angeles (LA) 001, Sayh al Uhaymir (SaU) 008, Shergotty, Tissint, and Zagami (Table 1). These meteorites were selected to include representatives from all three of the different geochemical groupings (depleted, intermediate, and enriched) observed in the shergottites (Borg et al., 2002) (Table 1). The samples also span the range of shock pressures and temperatures recorded (Fritz et al., 2005, 2017), and include meteorites recovered from all the terrestrial environments that meteorites can reside in prior to analysis, namely curated witnessed falls, hot desert finds, and Antarctic cold desert finds (Table 1, Fig. 3). Where available, we analyzed multiple phases from each sample (i.e., pyroxene, plagioclase glass, plagioclase glass rinsed in hydrofluoric acid, olivine, impact melt, and groundmass; Data file S1).

Six meteorites (DaG 476, LA 001, SaU 008, Shergotty, Tissint, and Zagami) were prepared and analyzed at the NERC Argon Isotope Facility of the Scottish Universities Environmental Research Centre (SUERC) and a seventh (ALH 77005) analyzed at the Berkeley Geochronology Center.

At SUERC, small samples of meteorites (<100 mg) located away from the fusion crust and/or signs of terrestrial weathering were gently crushed in an agate mortar and pestle to liberate individual mineral phases, which were then cleaned for a minimum of 60 minutes in deionized water plus ethanol in an ultrasonic bath at <50 °C. Selected fragments of plagioclase diaplectic glass (transparent glass formed via shock pressure-induced recrystallization of plagioclase, Fritz et al., 2019) were also etched for an additional 3 minutes in 5% hydrofluoric acid. Hand-picked fragments 250-500 μm in diameter (not weighed) were then loaded into 21-well aluminum disks along with three separate age standards: Fish Canyon sanidine (~125-250 μm) (Morgan et al., 2014), Hb3gr hornblende (125-160 μm) (Jourdan et al., 2006), and GA1550 biotite (250-500 μm) (McDougall and Wellman, 2011) for irradiation. The irradiation canister was vacuum-sealed in a quartz vial and irradiated for 20 hours in the Cd-lined TRIGA facility, Oregon State University, USA.

After a decay period of between 1.5 and 6 months, aliquots of the age standards and shergottite samples were placed in 2 mm diameter and 2 mm deep circular holes in a steel palette, which was loaded into a laser chamber of a noble gas ultrahigh vacuum extraction line and baked at <150 °C for ~2 days. Shergottite analyses were performed on aliquots comprising 2-6 fragments of 250-500 μm diameter, representing ca. 5-20 mg of material.

The samples at SUERC were analyzed on a MAP-215-50 mass spectrometer operated in peak-hopping mode, with a measured sensitivity of 6.5×10^{-15} moles/Volt. Fish Canyon and Hb3gr crystals were analyzed via total-fusion, while GA1550 and meteorite samples were incrementally heated using a using a defocused CO_2 laser. The released gases were purified using two SAES® GP-50 getters with ST101 Zr-Al cartridges, one at room temperature and the other at ~450 °C. Isotope extraction, purification, extraction line operation, and mass spectrometry were fully automated. Data were corrected for background measurements, mass discrimination, and radioactive decay since irradiation using *MassSpec* software version 8.131. Mass spectrometer discrimination per AMU was determined via analyses of n = 933 air aliquots over a period of nine months, and was calculated using the power law, and a terrestrial atmospheric $^{40}Ar/^{36}Ar$ value of 298.56 ± 0.31 (Lee et al., 2006), yielding a value of 1.00976 ± 0.00249 [1 s.d.]. For the neutron flux calculation (J parameter), we used the age for Fish Canyon sanidine of 28.294 ± 0.036 Ma (1σ) and ^{40}K decay constants from Renne et al. (2011); details of other decay constants and irradiation parameters are in Data file S1. All uncertainties in Data file S1 are reported at the one-sigma level, while all uncertainties in the text and figures are reported at the two-sigma level.

As an additional test of the robustness of our J values determined from the analyses of Fish Canyon sanidine (Jourdan and Renne, 2007; Morgan et al., 2014), we analyzed 14 aliquots of the international standard GA1550 biotite (McDougall and Wellman, 2011), and 12 aliquots of Hb3gr (Jourdan et al., 2006) as unknown samples. These GA1550 and Hb3gr analyses yielded weighted mean ages of 99.89 ± 0.22 Ma (2σ; n = 44), and 1082.1 ± 2.2 Ma (2σ; n = 12), respectively (Data file S1). These results are within uncertainty of the accepted ages for these samples, of 99.738 ± 0.208 Ma (2σ) (Renne et al., 2011), and 1081.0 ± 2.4 Ma (2σ) (Renne et al., 2011).

ALH 77005 was prepared and analyzed at the Berkeley Geochronology Center (BGC), USA. Three whole-rock fragments weighing ~11.5 mg (Aliquot 1), ~3.0 mg (Aliquot 2), and ~6.5 mg (Aliquot 3) were handpicked for analysis. The handpicked aliquots were irradiated for 100 hours in the Cd-lined TRIGA facility, Oregon State University, USA, alongside the Hb3gr fluence monitor. After a decay period of ~4.5 months, the samples were placed into Pt-Ir packets, loaded into an ultra-high vacuum laser chamber with a sapphire viewport, and heated with a 30 W diode laser equipped with an optical pyrometer (Shuster et al., 2010). The standards were fused in a single heating step using a CO_2 laser. The released argon was purified using one hot (~450 °C) and one cold (room temperature) SAES® GP-50 getter pump fitted with a C-50 cartridge (St101 alloy). Ar isotopes were analyzed statically using a Mass Analyzer Products 215c mass spectrometer in peak hopping mode on a Balzers SEV-217 electron multiplier. Gas extraction and analysis were fully automated.

BGC data were corrected for background measurements, mass discrimination, and radioactive decay since irradiation. Mass spectrometer discrimination per AMU was determined via analyses of terrestrial atmospheric Ar aliquots interspersed with analyses of ALH 77005 and was calculated using the power law and a terrestrial atmospheric $^{40}Ar/^{36}Ar$ value of 298.56 ± 0.31 (Lee et al., 2006), yielding a value of 1.00288 ± 0.00130 [1 s.d.]. Ages were calculated using the decay constants and standard calibration from Renne et al. (2011); details of other decay constants and irradiation parameters are in Data file S1. All uncertainties in Data file S1 are reported at the one-sigma level, while all uncertainties in the text and figures are reported at the two-sigma level.

We also determined cosmogenic exposure ages, as this age information was used to correct $^{40}Ar/^{39}Ar$ data for contributions of cosmogenic ^{38}Ar and ^{36}Ar (Cassata and Borg, 2016). The cosmogenic exposure age analyses were performed on unirradiated aliquots, with noble gas measurements undertaken at SUERC, following the same heating and gas extraction procedure as described

Table 1
$^{40}Ar/^{39}Ar$ ages and sample information for shergottites analyzed in this study.

Meteorite (geochemical type)	$^{40}Ar/^{39}Ar$ Age ± 2σ (Ma)	# of analyses in age	MSWD, p-value	Meteorite source & catalogue number	Max. Shock Δ Temp. (K)	Max. Shock Pressure (GPa)	Terrestrial residence time (years)	Fall/Find information
ALH 77005 (I)	-	-	-	Johnson Space Centre	800±200	45-55	200±70 ka	Find, 1977, Antarctica, 483 g
DaG 476 (D)	**481±24**	30	1.40, 0.076	NHM London, BM.2000,M7	470±100	40-45	60±20 ka	Find, 1998, Libya, 2015 g
LA 001 (E)	**170±47**	11	0.86, 0.563	NHM London, BM.2000,M12	560±120	45±3	<40 ka	Find, 1999, USA, 452.6 g
SaU 008 (D)	**437±24**	18	1.51, 0.087	NHM London, BM.2000,M39	470±100	40-45	NA	Find, 1999, Oman, 8580 g
Shergotty (E)	**161±9**	60	1.13, 0.228	NHM London, BM.1985,M171	100±50	20.5±2.5	150 years	Fall, 1865, India, 5000 g
Tissint (D)	**540±63**	29	1.02, 0.44	NHM London, BM.2012,M3	180-350	35-40	4 years	Fall, 2011, Morocco, 7000 g
Zagami (E)	**189±58**	24	0.19, 1.00	NHM London, BM.1993,M10	70±5	29.5±0.5	53 years	Fall, 1962, Nigeria, 18100 g

$^{40}Ar/^{39}Ar$ ages are 2σ full-external uncertainty, including the uncertainty in decay constants. Information about the meteorite geochemical type and fall/find information are from https://www.lpi.usra.edu/meteor/ and https://imca.cc/mars/martian-meteorites-list.htm. Abbreviations for geochemical type are: D, depleted; I, intermediate; E, enriched. Shock temperature and pressure data are from (Fritz et al., 2005, 2017; Hallis et al., 2017); terrestrial residence times for the witnessed falls (Shergotty, Tissint, and Zagami) were calculated as the time between the year of the fall and the year in which the samples were analyzed (in 2015); for ALH 77005 and DaG476 the data is from (Fritz et al., 2005) and LA 001 (Nishiizumi et al., 2000). NA: not available.

for the $^{40}Ar/^{39}Ar$ analyses. The aliquots for ^{38}Ar cosmogenic exposure analyses were taken from within a few millimetres of the $^{40}Ar/^{39}Ar$ fragments (usually ~2 mm, and always <5 mm), and so will have experienced a very similar flux of cosmogenic irradiation. As the ^{38}Ar cosmogenic isotope production rate is dependent on the concentrations of K, Ca, Fe, Ni, Ti, Cr, and Mn (Eugster and Michel, 1995), our ^{38}Ar production rates were determined by chemical analysis of the same fragments that were analyzed for cosmogenic argon, rather than by assuming a composition from published chemical analyses, in order to avoid complications that arise due to the analysis of small aliquots of heterogeneous samples. Chemical compositions of each sample (Table S2) were determined after the cosmogenic argon was extracted (i.e., on CO_2 laser-heated fused glass) by inductively coupled plasma mass spectrometry (ICP-MS) at Lawrence Livermore National Laboratory using the methods outlined in Wimpenny et al. (2019). Cosmogenic exposure ages were calculated from elemental production rates (Eugster and Michel, 1995). For these ^{38}Ar exposure age calculations, the relative contributions of trapped and cosmogenic Ar were determined by a two-component deconvolution assuming cosmogenic $^{38}Ar/^{36}Ar = 1.54$ (Wieler, 2002), and the trapped component is derived from the Martian atmosphere $^{38}Ar/^{36}Ar = 0.244$ (Wiens et al., 1986).

3. Results

Our ^{38}Ar cosmogenic exposure analyses yielded four distinct groups of ages: ~0.6-0.7 Ma for DaG 476 and SaU 008; ~1 Ma for Tissint; ~2.1-2.3 Ma for LA 001 and Shergotty; and ~2.7 Ma for Zagami (Table S2). These results are indistinguishable from published cosmogenic exposure ages from the respective meteorites, and confirm that these meteorites were ejected from Mars in separate events – and therefore at separate locations on Mars (Herzog and Caffee, 2014). ^{38}Ar cosmogenic exposure analyses were not undertaken for the meteorite ALH 77005; instead a literature age of 3.74 ± 0.85 Ma was used for this sample (Herzog and Caffee, 2014). These cosmogenic data were used to accurately correct our $^{40}Ar/^{39}Ar$ isotope data for cosmogenic ^{38}Ar and ^{36}Ar contributions, following the procedures of Cassata and Borg (2016).

The $^{40}Ar/^{39}Ar$ data are presented on isotope-correlation plots (Fig. 3). Analysis of multiple phases from the same rock increases the spread of data in $^{39}Ar/^{40}Ar$ versus $^{36}Ar/^{40}Ar$ (isotope correlation) space, thus improving the precision on both x and y intercepts (i.e., the age on the x-axis and the composition of trapped non-radiogenic argon on the y-axis) (Fig. 3). The isotope correlation plots show that the shergottite analyses typically define 'wedge-shaped' arrays (Fig. 3). To determine isochron ages for these samples, we used a modified 'sphenochron' approach (where 'sphen' [$\sigma\varphi\acute{\eta}\nu$] is the Greek word for 'wedge', Chen et al., 1996), with the isochron defined by the largest population of analyses that yield a statistically significant isochron (Mean Square of Weighted Deviates (MSWD) <2 and probability (p) of an MSWD higher than observed >5%) using either the highest or lowest $^{36}Ar/^{40}Ar$ ratio (i.e., the top or bottom of the wedge (Fig. 4)). All samples except ALH 77005 yielded an isochron that satisfied these criteria (Fig. 3).

As shown in Fig. 3, the y-intercepts of isochrons for the different meteorites define different initial trapped $^{40}Ar/^{36}Ar$ components. An explanation for the origin of these argon components is shown in Fig. 4. Tissint, Shergotty, Zagami, and LA 001 have $^{40}Ar/^{36}Ar$ intercepts that are indistinguishable from Martian atmosphere, as measured by Mars Science Laboratory Curiosity (1900 ± 600 (2σ)) (Mahaffy et al., 2013). Meanwhile, the samples DaG 476 and SaU 008 have $^{40}Ar/^{36}Ar$ intercepts that overlap with the terrestrial atmospheric value of 298.56 ± 0.31 (Lee et al., 2006). The data points that are statistical outliers from the isochrons (grey ellipses) for all samples clearly show variable mixing between the end members of terrestrial and Martian atmosphere (Fig. 3, 4). ALH 77005 contains a variable mixture of terrestrial and Martian atmospheric argon, but with neither end member being resolved, explaining why this sample did not yield an isochron. These results show that, although the shergottites formed on Mars, the terrestrial atmosphere has contaminated these meteorites during their residence on Earth.

The meteorites ALH 77005, DaG 476, and SaU 008 have been exposed to the terrestrial atmosphere for up to ca. 200,000 years (Table 1). The $^{40}Ar/^{39}Ar$ data shows that, for the meteorites that have resided on Earth for long durations, terrestrial atmospheric gas (which contains 1% argon, equivalent to a partial pressure of 1000 Pa) has entered the structure of the minerals, and now dominates with respect to any Martian atmospheric signal. Nevertheless, it is important to recognize that addition of terrestrial argon does *not* alter the $^{40}Ar/^{39}Ar$ isochron age (Fig. 4). This is because incorporation of terrestrial atmospheric argon (whether by adsorption, absorption, or diffusion) adds ^{40}Ar and ^{36}Ar to the rock (with a fixed ratio of 298.56, Lee et al., 2006), but does not cause radiogenic ^{40}Ar to be displaced or lost (Fig. 4). Radiogenic ^{40}Ar, which is the isotope used to calculate the sample's age, is only lost if the Martian rock phases (i.e., pyroxene, plagioclase glass, impact melt) are destroyed by some process (e.g., terrestrial weathering), and new minerals such as clays and carbonates are formed. Such terrestrially formed materials were avoided in this study by the adoption of rigorous sample preparation procedures. The results show that the meteorites recovered from both hot and cold

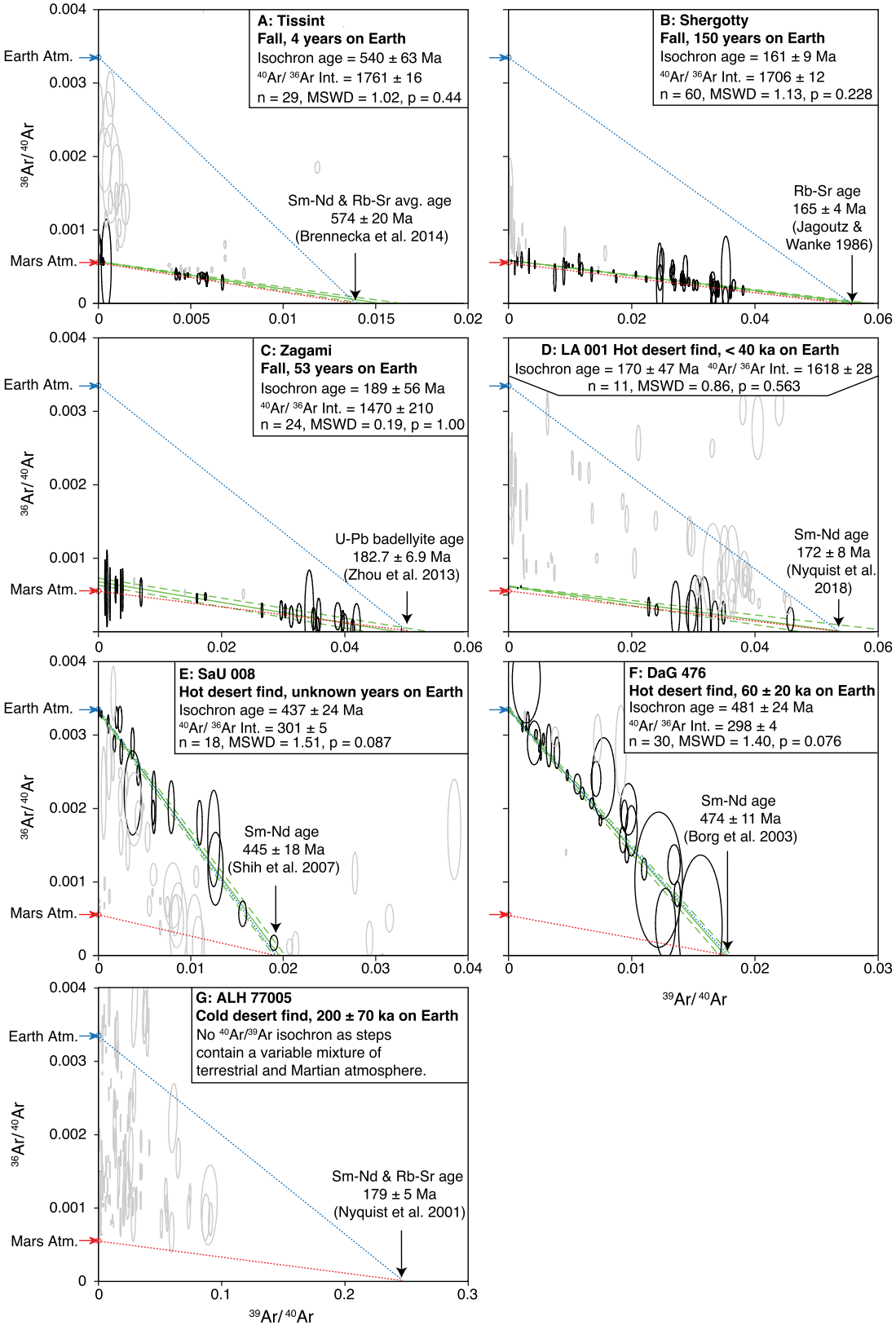

Fig. 3. $^{36}Ar/^{40}Ar$ vs. $^{39}Ar/^{40}Ar$ isotope correlation diagrams. **(A)** Tissint, **(B)** Shergotty, **(C)** Zagami, **(D)** LA 001, **(E)** SaU 008, **(F)** DaG 476, and **(G)** ALH 77005. Black ellipses are analyses that define statistically significant isochrons (green solid line, with 2σ envelope in dashed lines). Grey ellipses are analyses that are statistical outliers from the isochrons. Also plotted are the compositions for Earth atmosphere (blue arrow), Martian atmosphere (red arrow), and tie-lines representing hypothetical isochrons between these atmospheric constraints and the Sm-Nd, U-Pb, or Rb-Sr age for each sample (blue for the isochron leading to the terrestrial atmosphere, red for Martian atmosphere). Steps with negligible gas released and $^{36}Ar/^{40}Ar$ uncertainties of $>1 \times 10^{-3}$ were not plotted. The data were plotted using the MATLAB code in Data file S3. These diagrams incorporate data from all aliquots analyzed from each meteorite; for diagrams of the individual phases analyzed, see Data file S1.

deserts are affected by ingress of terrestrial atmospheric argon, indicating that the process of incorporating terrestrial argon still occurs at Antarctic temperatures (Fig. 3)(Schwenzer et al., 2009, 2013).

In contrast, it is notable – although not surprising – that the meteorite falls Shergotty, Zagami, and Tissint which fell to Earth in 1865, 1962, and 2011, respectively, preserve the highest $^{40}Ar/^{36}Ar$ values, corresponding with the Martian atmosphere. The rapid recovery of these three falls coupled with museum storage likely protected these meteorites from the worst effects of exposure and terrestrial atmosphere ingress. However, small amounts of terrestrial atmosphere have still been incorporated during their time on Earth. Even Tissint, which resided on Earth for only four years prior to analysis – the shortest duration of any shergottite – has some steps that contain admixed terrestrial argon (Fig. 3A). The admixed terrestrial argon was released during the low-temperature analyses of olivine (Data File S1), a mineral phase that contains little or no radiogenic argon, but is highly fractured (Balta et al., 2015), facilitating argon ingress. Any $^{40}Ar/^{36}Ar$ data from the shergottite meteorites must therefore be regarded as providing minimum values for Mars' atmosphere, although given the agreement in $^{40}Ar/^{36}Ar$ intercepts from Shergotty, Tissint, and Zagami, their intercepts are likely very close to the true Martian atmospheric value. LA 001 also yielded a Martian $^{40}Ar/^{36}Ar$ value, albeit with numerous data points also displaying ingress indicative of contamination with terrestrial atmosphere (Fig. 3D). This meteorite was reportedly found in the Mohave (a hot desert), and retains a well-preserved fusion crust with flow lines that indicates a relatively recent arrival to Earth, supported by a terrestrial residence age of $<$40 ka (Table 1, Nishiizumi et al., 2000).

We note from our analyses and previous work (Bogard et al., 1986) that the highest concentrations of Martian atmospheric argon are contained in impact melt glass (Data file S1). This observation is consistent with laboratory-based shock experiments of analogue materials, which demonstrate that impact melt glasses can trap significant amounts of Martian atmospheric argon at the time of impact (Wiens and Pepin, 1988). As the shergottites have a simple (one-stage) shock deformation history (Walton et al., 2008; Darling et al., 2016; Stöffler et al., 2018), this Martian atmospheric gas was trapped at the time of ejection into space.

The initial trapped $^{40}Ar/^{36}Ar$ components showing a Martian atmospheric signal for Shergotty and Zagami, and especially for Tissint ($^{40}Ar/^{36}Ar$ of 1761 $\pm$ 16; Fig. 3) are considerably more precise than the data from Curiosity (Mahaffy et al., 2013), which yielded a value of 1900 $\pm$ 600 (2σ). Our results are also an order of magnitude more precise than previous shergottite analyses (Bogard and Garrison, 1999; Avice et al., 2018), e.g., ALH 77005 $^{40}Ar/^{36}Ar$ of 1760 $\pm$ 200; EETA 79001 $^{40}Ar/^{36}Ar$ of 1735 $\pm$ 170; and Tissint $^{40}Ar/^{36}Ar$ of 1714 $\pm$ 340 [all quoted uncertainties are 2σ].

4. Discussion

$^{40}Ar/^{39}Ar$ dating of shergottites has historically proved challenging due to difficulties associated with resolving the different sources of argon that can be trapped within these rocks (Bogard et al., 2009; Korochantseva et al., 2009; Park et al., 2013b; Cassata and Borg, 2016), namely: (1) ^{40}Ar argon from the radioactive decay of ^{40}K (i.e., radiogenic argon, which is used to calculate the age); (2) ^{40}Ar, ^{38}Ar, and ^{36}Ar from the Martian atmosphere; (3) ^{38}Ar and ^{36}Ar produced from cosmogenic irradiation while the meteoroid was in space; (4) ^{40}Ar, ^{38}Ar, and ^{36}Ar from the terrestrial atmosphere; and lastly (5) ^{40}Ar, ^{39}Ar, ^{38}Ar, ^{37}Ar, and ^{36}Ar produced during laboratory neutron irradiation on Earth (an analytical step critical to the $^{40}Ar/^{39}Ar$ method). Previously published shergottite $^{40}Ar/^{39}Ar$ experiments have yielded argon isotope data that are difficult to interpret and has required invoking complex interpretive frameworks, which are underpinned by either 'parentless' or 'excess' argon contamination (Bogard and Garrison, 1999; Bogard et al., 2009; Korochantseva et al., 2009; Park et al., 2013a,b), or impact resetting (Bouvier et al., 2005, 2008; Jaret et al., 2018).

Unlike previous discordant $^{40}Ar/^{39}Ar$ data, our $^{40}Ar/^{39}Ar$ isochron ages are concordant with the shergottite ages determined by the Sm-Nd, U-Pb, Rb-Sr, or Lu-Hf chronometers (Fig. 1B, 3). We propose three main reasons for the concordance, which contrasts with previous $^{40}Ar/^{39}Ar$ studies (Fig. 1A). Firstly, our use of the data reduction procedure of Cassata and Borg (2016) allows for accurate resolution of and correction for cosmogenic argon (a previously uncorrected or under-corrected Ar reservoir). Secondly, isotope correlation plots are used to define the initial trapped $^{40}Ar/^{36}Ar$ components for each meteorite, rather than forcing an assumed $^{40}Ar/^{36}Ar$ ratio onto the data. This is important, as instead of making assumptions about the geological context and Ar systematics of the shergottite meteorites, we allow the data to constrain the trapped $^{40}Ar/^{36}Ar$ values; our data demonstrates that the shergottite meteorites contain variable proportions of Martian and terrestrial atmosphere. Thirdly, the rigorous sample preparation, involving analysis of multiple mineral separates wherever possible (pyroxene, plagioclase glass, plagioclase glass rinsed in hydrofluoric acid, olivine, impact melt, and/or groundmass), increases the spread of data on the isotope correlation plots, allowing improved precision of axis-intercepts and improving the utility of the isochron data. As is apparent from the isotope correlation diagrams (Fig. 3, 4, Data file S1), many of the data points contain admixed terrestrial and Martian atmospheric argon. For any such points, the 'model' ages calculated using a fixed value for trapped argon (either terrestrial or Martian atmosphere – an approach used by many previous $^{40}Ar/^{36}Ar$ studies of the shergottites) would yield results with no geological significance (Data File S1).

Prior to this study, DaG 476, LA 001, SaU 008, Shergotty, Tissint, and Zagami all yielded $^{40}Ar/^{39}Ar$ ages older than the other radioisotopic chronometers (Fig. 1A, Table S1). This discordance is now resolved (Fig. 1B, 3, 4): all of the argon present in these samples is either radiogenic, cosmogenic, or from Martian $\pm$ terrestrial atmospheres, and there is no evidence for 'parentless' or 'excess' argon (Bogard and Garrison, 1999; Bogard et al., 2009; Korochantseva et al., 2009; Park et al., 2013a,b). Our data support interpretation that the shergottites sample the youngest volcanoes on Mars (McSween and McLennan, 2014; Herd et al., 2017; Lapen et al., 2017). However, given that the shergottites experienced shock metamorphism, it could be considered surprising that the $^{40}Ar/^{39}Ar$ age data overlap with ages from other high closure temperature chronometers. We contend the physical properties of the shergottites, such as the minerals, glasses and textures formed by shock metamorphism, support our data and interpretation.

The shergottite meteorites experienced a variety of shock conditions. For example, the maximum shock temperature experienced by Zagami was only 70 $\pm$ 5 °C above ambient, and the bulk of Shergotty experienced heating of just 100 $\pm$ 50 °C above ambient (Fritz et al., 2005), where Martian ambient surface temperatures are typically well below freezing (averaging −60 °C). Heating to these temperatures – regardless of duration – would not induce significant Ar diffusion in mafic igneous rocks (Cassata et al., 2011; Cassata and Renne, 2013), let alone influence the isotopic systems with closure temperatures in excess of 800 °C, such as the Sm-Nd system, or U-Pb in zircon and baddeleyite (Reiners et al., 2018). Most shergottite meteorites do contain diaplectic glass formed by shock metamorphism of plagioclase, but it is crucial to emphasize that the presence of diaplectic glass does not by itself indicate high temperatures; laboratory-based shock experiments (undertaken at 20 °C and *minus* 196 °C) demonstrate that diaplectic plagioclase glass can readily form at typical Martian surface temperatures,

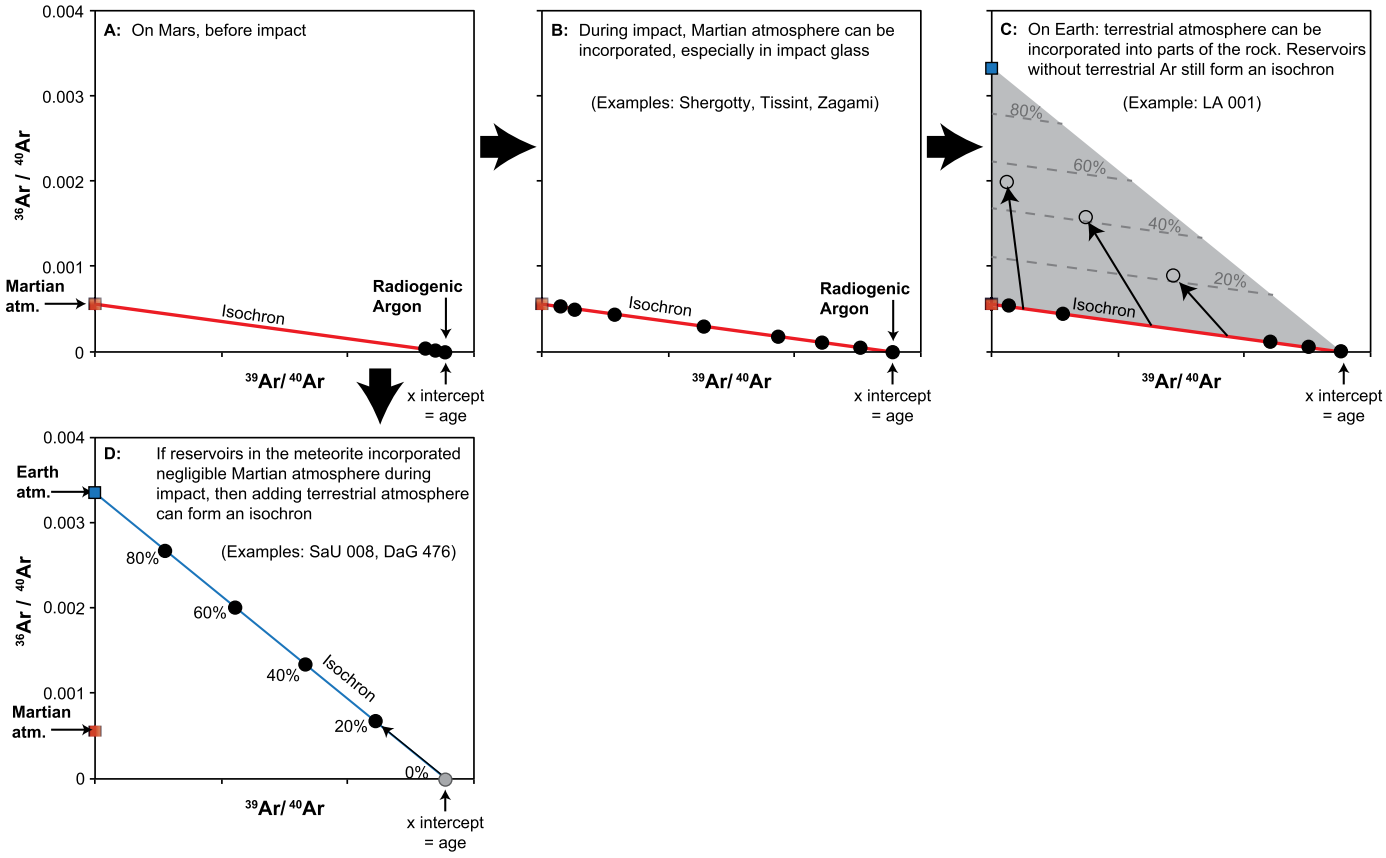

Fig. 4. Schematic diagrams demonstrating the sequence of events that affected argon in Martian meteorites. (**A**) On Mars, due to the decay of ^{40}K into ^{40}Ar, an igneous rock hundreds of million years old will contain nearly 100% radiogenic Ar with a small amount of Martian atmosphere. This is what the results should look like from a hypothetical analysis on an unshocked lava obtained by a sample-return mission or analyzed on Mars. (**B**) During the impact that ejected the meteorite into space, additional Martian atmosphere can be shock-implanted into the rock. Gas with variable mixtures of the two components (black dots) will lie on an isochron (red line), with the intercepts corresponding to radiogenic argon and the Martian atmosphere. (**C**) Once on Earth, terrestrial atmosphere can become incorporated (black arrows trending towards the blue square, with grey dashed lines indicating the percentage of added terrestrial atmosphere). Analyses with a three-component mixture will fall within the grey wedge, with the vertices representing radiogenic argon, Martian atmosphere, and Earth atmosphere. (**D**) A special case will occur if a reservoir that initially contained only radiogenic argon (i.e., negligible Martian atmosphere) has terrestrial argon added. In this case, the isochron will trend between radiogenic argon and terrestrial atmosphere. Crucially, in all four scenarios (**A-D**), the x-intercept yields the samples' ^{40}Ar/^{39}Ar age, regardless of the amount of Martian or terrestrial atmosphere incorporated.

without heating (Fritz et al., 2019). The presence of plagioclase diaplectic glass in the shergottites is therefore indicative of high shock pressures only, and *not* necessarily high temperatures (Fritz et al., 2019).

Some shergottites have experienced more intense shock heating, for example opaque impact melt glass in Shergotty and Tissint indicates conditions hot enough to melt localized portions of these meteorites (Fritz et al., 2005, 2017) – with temperatures of 2000 °C proposed (Baziotis et al., 2013). Crucially, the preservation of high-pressure phases within the shock melt glasses indicate that these melts were quenched rapidly – in the order of 1 second or less (Walton et al., 2014; Hu and Sharp, 2017) – which is too fast for significant Ar diffusion to occur out of the glass. From the perspective of ^{40}Ar/^{39}Ar geochronology, even if heating or melting occurs, if the Ar does not have time to diffuse out of the rock (e.g., due to rapid quenching), then the Ar clock will not be reset, and the sample will retain the original cooling age of igneous crystallization.

The effects of such shock heating are also highly heterogeneous and localized; away from the shock melt pockets, the mineralogy and textures within the shergottites indicate that the bulk of these samples experienced temperatures of up to 180-350 °C above ambient for Tissint, 470 ± 100 °C for DaG 476 and SaU 005, 560 ± 120 °C for LA 001, and 800 ± 200 °C for ALH 77005 (Fritz et al., 2005) (Table 1). Such temperatures have the potential to induce Ar loss, but only if these temperatures were maintained for sufficiently long durations (Cassata et al., 2011; Cassata and Renne, 2013). Therefore, to examine the effect of such shock heating and quantify the potential for Ar loss, we have modelled the cooling history of the shergottites following such a thermal disturbance (Fig. 5).

The shock-formed phases and textures within the shergottites indicate the meteorites experienced only one episode of shock metamorphism: the impact event that ejected the specimens from the Martian surface (Darling et al., 2016; Stöffler et al., 2018; Hu et al., 2023). This simplifies modelling, as it enables the cooling behaviour to be modelled in 3D as spheres of rock starting at a uniform initial temperature. The MATLAB code for these calculations is contained in Data file S2. The meteorites were modelled with radii of 0.2 and 0.3 m (diameters of 0.4 and 0.6 m) – these dimensions were determined from cosmogenic isotope exposure analyses, and represent the original size of the shergottite meteorites when they were ejected from Mars (Goswami et al., 1997; Eugster et al., 2002) (i.e., before passage through the terrestrial atmosphere, when meteorites loose considerable mass). Temperatures of 100, 400, and 800 °C were used as they match the observed shock temperatures within the solid portions of the shergottites (Table 1); the higher temperatures of up to 2000 °C were only experienced by very small and localized melt pockets within the meteorites, which as mentioned above were quenched in <1 second (Fritz et al., 2005; Baziotis et al., 2013; Walton et al., 2014;

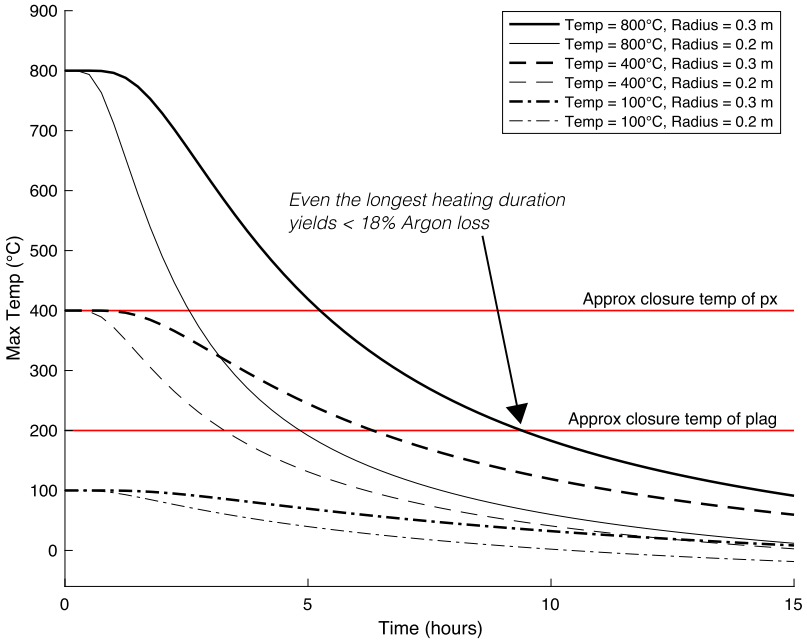

Fig. 5. Thermal modelling of shergottites after shock heating and ejection into space. These curves are from cooling models of the centre of the meteorite (the slowest part to cool), for diameters of 40 and 60 cm and initial shock heating temperatures of 100, 400, and 800 °C. Horizontal red lines at 400 and 200 °C denote the approximate closure temperatures for pyroxene and plagioclase, respectively. Some shergottites (like Zagami and Shergotty) were never heated above 100 °C, so would never have been above the closure temperature of plagioclase, These models also show that even the largest, most shock-heated shergottites would have experienced less than 10 hours of argon diffusion for plagioclase and 5 hours for pyroxene, leading to negligible (<4-18%) Ar loss (Weiss et al., 2002). Code for these calculations is contained in Data file S2.

Fritz et al., 2017; Hu and Sharp, 2017). Shock heating due to pore compression (Bland et al., 2014; Jourdan et al., 2017) is expected to be minimal in the shergottites due to their crystalline nature with no or negligible porosity.

The spheres were surrounded by the vacuum of space at a constant temperature of −60 °C, which is based on average temperatures near Mars (McKay et al., 1991; Weiss et al., 2002). We did not model the time the meteoroid spent in the Martian atmosphere, which is on the order of 2 seconds or less (i.e., a 10 km thick atmosphere and escape velocity of 5 km/s), and therefore negligible on the timescale of cooling. Also, by analogy with terrestrial meteorites which are cool to the touch when they land, frictional heat generated during passage through the Martian atmosphere would be lost by ablation of the outer portion of the meteoroid. Within the meteorites, we modelled heat diffusion using a thermal diffusivity of 10^{-6} m^2/s, a representative value for mafic igneous rocks. At the surface of the meteorites, we assumed heat radiated into space according to the Stefan-Boltzmann law, using a surface emissivity of 0.93 (Weiss et al., 2002) and specific heat capacity of 815 J/kg/K (Weiss et al., 2002). Because the meteorites were travelling through space at considerable velocity (several km/s), heat lost through radiation was removed from the system; it was not modelled as heating the surrounding vacuum, which was constantly being replaced as the meteorites moved.

The system of differential equations was solved by finite difference methods using the explicit Runge-Kutta pair of orders 2 and 3 of Bogacki and Shampine (MATLAB ODE solver ode23) (Shampine and Reichelt, 1997). This lower order solver was more efficient than the medium order MATLAB solver ode45 using the explicit Runge-Kutta pair of orders 4 and 5 of Dormand and Prince (Shampine and Reichelt, 1997), but the cooling times differed by <0.0005%. The system was modelled using a resolution of 0.005 m in all three dimensions. Resolution testing showed that increasing the resolution to 0.004 m, which doubles the total number of cells in the model, changed the time for a 0.3 m radius meteorite with a shock heating temperature of 400 °C to cool to 200 °C by <0.25%. The effect of the increased resolution would be smaller for smaller meteorites, higher shock heating temperatures, or higher closure temperatures.

Our thermal models demonstrate that following impact-ejection the shergottites cooled rapidly: even a meteorite heated to the highest temperature observed in the shock metamorphic minerals (800 °C) with the largest diameter of ~60 cm (Goswami et al., 1997; Eugster et al., 2002) cools to below 400 °C in just over 5 hours and to 200 °C in under 10 hours (Fig. 5). These models represent the limiting upper bound on the extent of heating, as the models are for spherical meteorites, and any deviations from a sphere (e.g., an irregular or elongated shape) would increase the surface to volume ratio, causing the meteorite to cool faster. Also, the cooling times shown are for material at the centre of the meteorites – material closer to the edge cools more rapidly.

Diffusion modelling shows that plagioclase, the mineral in shergottites with the highest diffusivity, experiences <4-18% argon loss when subjected to these temperature-time conditions of shock metamorphism (Weiss et al., 2002). This is consistent with the analytical results: for four meteorites (ALH 77005, LA 001, SaU 008, and Tissint, which all experienced shock heating above the closure temperature of argon in plagioclase, Table 1), there are a small number of datapoints that plot to the right of the main 'wedge' of analyses (Fig. 3). Steps that plot in this region of the isotope correlation diagrams correspond to $^{40}Ar/^{39}Ar$ ages that are younger than the samples' respective Sm-Nd, Rb-Sr, or U-Pb ages, indicating argon loss; these steps are not used to calculate the $^{40}Ar/^{39}Ar$ isochron ages. We highlight that these results confirm that the degree of argon loss is minor, as only a few steps are affected. Thus, we conclude that, due to the brief time spent at elevated temperatures, the shergottites considered here would have experienced minor to negligible argon loss, and that the analytical steps demonstrably influenced by argon loss are excluded from our age calculations by the isochron approach. These observations are consistent with previous studies of shock heating and argon diffusion in meteorites (Weiss et al., 2002; Fritz et al., 2005; Shuster et al., 2010). Significant argon diffusion can occur if the mafic target rocks are completely melted and kept molten, as argon diffusion

out of a melt is significantly faster than out of solid minerals (e.g., the Lonar crater on Earth, Jourdan et al., 2011). The shergottite meteorites, however, did not experience near-complete melting, but instead contain (at most) rare areas of rapidly quenched melt.

We note that shock-metamorphosed (but unmelted) rocks within terrestrial impact craters have been used as analogues for the shergottite meteorites, for example maskelynite-bearing mafic rocks at the Manicouagan crater, Canada (Jaret et al., 2018). These terrestrial impact rocks have yielded $^{40}Ar/^{39}Ar$ ages fully or partially reset by impact, leading to interpretations that the shock-metamorphosed shergottites were similarly reset (Jaret et al., 2018). However, we emphasize that meteorites ejected into space by impacts experience very different temperature-time paths compared to shock-metamorphosed but unmelted material that remains on the planet within impact crater deposits. In contrast to meteorites that cool within minutes to hours (Fig. 5), these planet-bound impact deposits are insulated by the surrounding material, and remain at elevated temperatures ($\gg 200\,^{\circ}C$) for tens of thousands to a few million years (Abramov and Kring, 2007), allowing the time necessary for argon diffusion to fully or partially reset the $^{40}Ar/^{39}Ar$ system (Jourdan et al., 2007). Thus, in terms of Ar-isotope systematics, terrestrial shock-metamorphosed impact crater deposits are poor $^{40}Ar/^{39}Ar$ analogues for meteorites, as the cooling timescale differs by eight to ten orders of magnitude.

5. Conclusions

On Earth, $^{40}Ar/^{39}Ar$ is the most widely applied and versatile geochronologic technique applied to mafic igneous rocks. $^{40}Ar/^{39}Ar$ should be similarly useful for Martian samples, including the shergottites. Until now this has not been the case, with $^{40}Ar/^{39}Ar$ previously yielding highly inconsistent ages for individual meteorites, with results that are discordant and typically older compared to other geochronometers (Fig. 1). In contrast, our $^{40}Ar/^{39}Ar$ results are synchronous with the U-Pb, Sm-Nd, and Rb-Sr ages for the meteorites studied, demonstrating that the $^{40}Ar/^{39}Ar$ method can successfully yield accurate igneous formation ages for the shergottite meteorites. Our results support interpretations that the Pb-Pb model ages of >4000 Ma likely reflect ancient Martian mantle differentiation events (Bellucci et al., 2016), and not cooling ages for magma eruption or intrusion. Despite undergoing shock metamorphism, most of the shergottite minerals experienced minor to negligible argon loss owing to the lack of or brief time at elevated temperatures. Their magmatic cooling ages have thus been retained, and not substantially reset by shock. Shock-metamorphosed samples from terrestrial impact structures are poor $^{40}Ar/^{39}Ar$ analogues for meteorites ejected into space as the cooling timescale differs by eight to ten orders of magnitude.

Our shergottite $^{40}Ar/^{39}Ar$ ages range from 161 ± 9 Ma to 540 ± 63 Ma (2σ), indicating that these meteorites are sourced from the most recent volcanoes on Mars, which are the largest such edifices in the Solar System. This conclusion is consistent with modelling of meteorite spallation (Head et al., 2002), which strongly favours ejection of rocks from the younger Martian terrains that have the thinnest coatings of regolith. Evidence for ingress of terrestrial atmosphere into these extra-terrestrial samples during their time on Earth emphasizes the importance of strict sample protection protocols for samples returned from Mars (Beaty et al., 2019). Alternatively, rover-based dating of materials on the Martian surface would bypass the complications of terrestrial contamination (Morgan et al., 2017). The analytical techniques and data regression procedures used in this study are critical to establish robust protocols for reliable $^{40}Ar/^{39}Ar$ analyses applied to sample-return material from Mars.

CRediT authorship contribution statement

Benjamin E. Cohen: Writing – original draft, Writing – review & editing, Visualization, Resources, Methodology, Investigation, Formal analysis, Data curation, Conceptualization. **Darren F. Mark:** Writing – original draft, Writing – review & editing, Validation, Resources, Project administration, Methodology, Investigation, Funding acquisition, Formal analysis, Conceptualization. **William S. Cassata:** Writing – review & editing, Validation, Software, Resources, Methodology, Investigation, Funding acquisition, Data curation. **Lara M. Kalnins:** Writing – review & editing, Visualization, Validation, Software, Investigation, Formal analysis. **Martin R. Lee:** Writing – review & editing, Project administration, Methodology, Funding acquisition, Conceptualization. **Caroline L. Smith:** Writing – review & editing, Resources, Funding acquisition, Data curation, Conceptualization. **David L. Shuster:** Writing – review & editing, Validation, Investigation, Formal analysis.

Declaration of competing interest

The authors declare that they have no competing interests.

Data availability

The authors declare that all data supporting the findings of this study are included in this published article and its supplementary information files.

Acknowledgements

We thank the Natural History Museum London and the Johnson Space Centre for the provision of shergottite samples. R. Dymock and J. Imlach (SUERC) assisted with $^{40}Ar/^{39}Ar$, and Josh Wimpenny (LLNL) with ICP-MS analyses. We thank Jörg Fritz for discussions on shock metamorphism, Fred Jourdan and anonymous referees for reviews. This work was funded by the UK Science and Technology Facilities Council (grants ST/H002960/1, and ST/K000918/1 to D.F.M. and M.R.L.). W.S.C. was supported by the NASA Mars Fundamental Research Program (grant NNH14AX56I) and an LLNL Laboratory Directed Research and Development project (20-LW-008). Portions of this work were performed under the auspices of the U.S. Department of Energy by Lawrence Livermore National Laboratory under Contract DE-AC52-07NA27344. L.M.K. is supported by a Royal Society of Edinburgh Personal Research Fellowship funded by the Scottish Government. D.L.S. was supported by the Ann and Gordon Getty Foundation. NERC are thanked for continued funding of the Argon Isotope Facility at SUERC. The project was developed by B.E.C., D.F.M., and M.R.L.; samples were selected by C.L.S., D.F.M., D.L.S., and W.S.C.; samples were prepared by B.E.C., D.L.S., and W.S.C.; analyses and $^{40}Ar/^{39}Ar$ data interpretation were undertaken by B.E.C., W.S.C., D.F.M., and D.L.S.; the thermal models and code for isotope correlation diagrams were prepared by L.M.K.; and manuscript prepared by B.E.C. and D.F.M. with contributions from all authors.

Appendix A. Supplementary material

Supplementary material related to this article can be found online at https://doi.org/10.1016/j.epsl.2023.118373.

References

Abramov, O., Kring, D.A., 2007. Numerical modeling of impact-induced hydrothermal activity at the Chicxulub crater. Meteorit. Planet. Sci. 42, 93–112.

Avice, G., Bekaert, D.V., Chennaoui Aoudjehane, H., Marty, B., 2018. Noble gases and nitrogen in Tissint reveal the composition of the Mars atmosphere. Geochem. Perspect. Lett. 11 (16). https://doi.org/10.7185/geochemlet.1802.

Balta, J.B., Sanborn, M.E., Udry, A., Wadhwa, M., McSween, H.Y., 2015. Petrology and trace element geochemistry of Tissint, the newest shergottite fall. Meteorit. Planet. Sci. 50, 63–85. https://doi.org/10.1111/maps.12403.

Baziotis, I.P., Liu, Y., DeCarli, P.S., Melosh, H.J., McSween, H.Y., Bodnar, R.J., Taylor, L.A., 2013. The Tissint Martian meteorite as evidence for the largest impact excavation. Nat. Commun. 4, 1404. https://doi.org/10.1038/ncomms2414.

Beaty, D.W., Grady, M.M., McSween, H.Y., Sefton-Nash, E., Carrier, B.L., Altieri, F., Amelin, Y., Ammannito, E., Anand, M., Benning, L.G., Bishop, J.L., Borg, L.E., Boucher, D., Brucato, J.R., Busemann, H., Campbell, K.A., Czaja, A.D., Debaille, V., Des Marais, D.J., Dixon, M., Ehlmann, B.L., Farmer, J.D., Fernandez-Remolar, D.C., Filiberto, J., Fogarty, J., Glavin, D.P., Goreva, Y.S., Hallis, L.J., Harrington, A.D., Hausrath, E.M., Herd, C.D.K., Horgan, B., Humayun, M., Kleine, T., Kleinhenz, J., Mackelprang, R., Mangold, N., Mayhew, L.E., McCoy, J.T., McCubbin, F.M., McLennan, S.M., Moser, D.E., Moynier, F., Mustard, J.F., Niles, P.B., Ori, G.G., Raulin, F., Rettberg, P., Rucker, M.A., Schmitz, N., Schwenzer, S.P., Sephton, M.A., Shaheen, R., Sharp, Z.D., Shuster, D.L., Siljeström, S., Smith, C.L., Spry, J.A., Steele, A., Swindle, T.D., ten Kate, I.L., Tosca, N.J., Usui, T., Van Kranendonk, M.J., Wadhwa, M., Weiss, B.P., Werner, S.C., Westall, F., Wheeler, R.M., Zipfel, J., Zorzano, M.P., 2019. The potential science and engineering value of samples delivered to Earth by Mars sample return. Meteorit. Planet. Sci. 54, S3–S152. https://doi.org/10.1111/maps.13242.

Bellucci, J.J., Nemchin, A.A., Whitehouse, M.J., Snape, J.F., Kielman, R.B., Bland, P.A., Benedix, G.K., 2016. A Pb isotopic resolution to the Martian meteorite age paradox. Earth Planet. Sci. Lett. 433, 241–248. https://doi.org/10.1016/j.epsl.2015.11.004.

Bland, P.A., Collins, G.S., Davison, T.M., Abreu, N.M., Ciesla, F.J., Muxworthy, A.R., Moore, J., 2014. Pressure–temperature evolution of primordial solar system solids during impact-induced compaction. Nat. Commun. 5, 5451. https://doi.org/10.1038/ncomms6451.

Bogard, D.D., Garrison, D.H., 1999. Argon-39-argon-40 "ages" and trapped argon in Martian shergottites, Chassigny, and Allan Hills 84001. Meteorit. Planet. Sci. 34, 451–473.

Bogard, D.D., Hörz, F., Johnson, P.H., 1986. Shock-implanted noble gases: an experimental study with implications for the origin of Martian gases in shergottite meteorites. J. Geophys. Res. 91, E99–E114.

Bogard, D.D., Park, J., 2008. ^{39}Ar-^{40}Ar dating of the Zagami Martian shergottite and implications for magma origin of excess ^{40}Ar. Meteorit. Planet. Sci. 43, 1113–1126.

Bogard, D.D., Park, J., Garrison, D., 2009. ^{39}Ar-^{40}Ar "ages" and origin of excess ^{40}Ar in Martian shergottites. Meteorit. Planet. Sci. 44, 905–923.

Borg, L.E., Brennecka, G.A., Symes, S.J.K., 2016. Accretion timescale and impact history of Mars deduced from the isotopic systematics of martian meteorites. Geochim. Cosmochim. Acta 175, 150–167. https://doi.org/10.1016/j.gca.2015.12.002.

Borg, L.E., Nyquist, L.E., Wiesmann, H., Reese, Y., 2002. Constraints on the petrogenesis of Martian meteorites from the Rb-Sr and Sm-Nd isotopic systematics of the lherzolitic shergottites ALH77005 and LEW88516. Geochim. Cosmochim. Acta 66, 2037–2053.

Bouvier, A., Blichert-Toft, J., Vervoort, J.D., Albarède, F., 2005. The age of SNC meteorites and the antiquity of the Martian surface. Earth Planet. Sci. Lett. 240, 221–233. https://doi.org/10.1016/j.epsl.2005.09.007.

Bouvier, A., Blichert-Toft, J., Vervoort, J.D., Gillet, P., Albarède, F., 2008. The case for old basaltic shergottites. Earth Planet. Sci. Lett. 266, 105–124. https://doi.org/10.1016/j.epsl.2007.11.006.

Cassata, W.S., Borg, L.E., 2016. A new approach to cosmogenic corrections in ^{40}Ar/^{39}Ar chronometry: implications for the ages of Martian meteorites. Geochim. Cosmochim. Acta 187, 279–293. https://doi.org/10.1016/j.gca.2016.04.045.

Cassata, W.S., Renne, P.R., 2013. Systematic variations of argon diffusion in feldspars and implications for thermochronometry. Geochim. Cosmochim. Acta 112, 251–287. https://doi.org/10.1016/j.gca.2013.02.030.

Cassata, W.S., Renne, P.R., Shuster, D.L., 2011. Argon diffusion in pyroxenes: implications for thermochronometry and mantle degassing. Earth Planet. Sci. Lett. 304, 407–416. https://doi.org/10.1016/j.epsl.2011.02.019.

Chen, Y., Smith, P.E., Evensen, N.M., York, D., Lajoie, K.R., 1996. The edge of time: dating young volcanic ash layers with the ^{40}Ar/^{39}Ar laser probe. Science 274, 1176–1178.

Christensen, P.R., Gorelick, N.S., Mehall, G.L., Murray, K.C., 2004. THEMIS Public Data Releases, Planetary Data System Node. Arizona State University. http://themis-data.asu.edu.

Darling, J.R., Moser, D.E., Barker, I.R., Tait, K.T., Chamberlain, K.R., Schmitt, A.K., Hyde, B.C., 2016. Variable microstructural response of baddeleyite to shock metamorphism in young basaltic shergottite NWA 5298 and improved U–Pb dating of Solar System events. Earth Planet. Sci. Lett. 444, 1–12. https://doi.org/10.1016/j.epsl.2016.03.032.

El Goresy, A., Gillet, P., Miyahara, M., Ohtani, E., Ozawa, S., Beck, P., Montagnac, G., 2013. Shock-induced deformation of Shergottites: shock-pressures and perturbations of magmatic ages on Mars. Geochim. Cosmochim. Acta 101, 233–262. https://doi.org/10.1016/j.gca.2012.10.002.

Eugster, O., Busemann, H., Lorenzetti, S., Terribilini, D., 2002. Ejection ages from krypton-81-krypton-83 dating and pre-atmospheric sizes of martian meteorites. Meteorit. Planet. Sci. 37, 1345–1360.

Eugster, O., Michel, T., 1995. Common asteroid break-up events of eucrites, diogenites, and howardites and cosmic-ray production rates for noble gases in achondrites. Geochim. Cosmochim. Acta 59, 177–199.

Farley, K.A., Stack, K.M., Shuster, D.L., Horgan, B.H.N., Hurowitz, J.A., Tarnas, J.D., Simon, J.I., Sun, V.Z., Scheller, E.L., Moore, K.R., McLennan, S.M., Vasconcelos, P.M., Wiens, R.C., Treiman, A.H., Mayhew, L.E., Beyssac, O., Kizovski, T.V., Tosca, N.J., Williford, K.H., Crumpler, L.S., Beegle, L.W., Bell III, J.F., Ehlmann, B.L., Liu, Y., Maki, J.N., Schmidt, M.E., Allwood, A.C., Amundsen, H.E.F., Bhartia, R., Bosak, T., Brown, A.J., Clark, B.C., Cousin, A., Forni, O., Gabriel, T.S.J., Goreva, Y., Gupta, S., Hamran, S.E., Herd, C.D.K., Hickman-Lewis, K., Johnson, J.R., Kah, L.C., Kelemen, P.B., Kinch, K.B., Mandon, L., Mangold, N., Quantin-Nataf, C., Rice, M.S., Russell, P.S., Sharma, S., Siljestrom, S., Steele, A., Sullivan, R., Wadhwa, M., Weiss, B.P., Williams, A.J., Wogsland, B.V., Willis, P.A., Acosta-Maeda, T.A., Beck, P., Benzerara, K., Bernard, S., Burton, A.S., Cardarelli, E.L., Chide, B., Clave, E., Cloutis, E.A., Cohen, B.A., Czaja, A.D., Debaille, V., Dehouck, E., Fairen, A.G., Flannery, D.T., Fleron, S.Z., Fouchet, T., Frydenvang, J., Garczynski, B.J., Gibbons, E.F., Hausrath, E.M., Hayes, A.G., Henneke, J., Jorgensen, J.L., Kelly, E.M., Lasue, J., Le Mouelic, S., Madariaga, J.M., Maurice, S., Merusi, M., Meslin, P.Y., Milkovich, S.M., Million, C.C., Moeller, R.C., Nunez, J.I., Ollila, A.M., Paar, G., Paige, D.A., Pedersen, D.A.K., Pilleri, P., Pilorget, C., Pinet, P.C., Rice Jr., J.W., Royer, C., Sautter, V., Schulte, M., Sephton, M.A., Sharma, S.K., Sholes, S.F., Spanovich, N., St Clair, M., Tate, C.D., Uckert, K., VanBommel, S.J., Yanchilina, A.G., Zorzano, M.P., 2022. Aqueously altered igneous rocks sampled on the floor of Jezero crater, Mars. Science 377, eabo2196. https://doi.org/10.1126/science.abo2196.

Fritz, J., Artemieva, N., Greshake, A., 2005. Ejection of Martian meteorites. Meteorit. Planet. Sci. 40, 1393–1411.

Fritz, J., Assis Fernandes, V., Greshake, A., Holzwarth, A., Böttger, U., 2019. On the formation of diaplectic glass: shock and thermal experiments with plagioclase of different chemical compositions. Meteorit. Planet. Sci. 54, 1533–1547. https://doi.org/10.1111/maps.13289.

Fritz, J., Greshake, A., Fernandes, V.A., 2017. Revising the shock classification of meteorites. Meteorit. Planet. Sci. 52, 1216–1232. https://doi.org/10.1111/maps.12845.

Goswami, J.N., Sinha, N., Murty, S.V.S., Mohapatra, R.K., Clement, C.J., 1997. Nuclear tracks and light noble gases in Allan Hills 84001: preatmospheric size, fall characteristics, cosmic-ray exposure duration and formation age. Meteorit. Planet. Sci. 32, 91–96.

Hallis, L.J., Huss, G.R., Nagashima, K., Taylor, G.J., Stöffler, D., Smith, C.L., Lee, M.R., 2017. Effects of shock and Martian alteration on Tissint hydrogen isotope ratios and water content. Geochim. Cosmochim. Acta 200, 280–294. https://doi.org/10.1016/j.gca.2016.12.035.

Head, J.N., Melosh, H.J., Ivanov, B.A., 2002. Martian meteorite launch: high-speed ejecta from small craters. Science 298, 1752–1756. https://doi.org/10.1126/science.1077483.

Herd, C.D.K., Walton, E.L., Agee, C.B., Muttik, N., Ziegler, K., Shearer, C.K., Bell, A.S., Santos, A.R., Burger, P.V., Simon, J.I., Tappa, M.J., McCubbin, F.M., Gattacceca, J., Lagroix, F., Sanborn, M.E., Yin, Q.-Z., Cassata, W.S., Borg, L.E., Lindvall, R.E., Kruijer, T.S., Brennecka, G.A., Kleine, T., Nishiizumi, K., Caffee, M.W., 2017. The Northwest Africa 8159 martian meteorite: expanding the martian sample suite to the early Amazonian. Geochim. Cosmochim. Acta 218, 1–26. https://doi.org/10.1016/j.gca.2017.08.037.

Herzog, G.F., Caffee, M.W., 2014. Cosmic-ray exposure ages of meteorites. In: Davis, A.M. (Ed.), Treatise on Geochemistry, 2nd edition. Elsevier, Amsterdam, pp. 419–454.

Hu, J., Asimow, P.D., Liu, Y., Ma, C., 2023. Shock-recovered maskelynite indicates low-pressure ejection of shergottites from Mars. Sci. Adv. 9, eadf2906. https://doi.org/10.1126/sciadv.adf2906.

Hu, J., Sharp, T.G., 2017. Back-transformation of high-pressure minerals in shocked chondrites: low-pressure mineral evidence for strong shock. Geochim. Cosmochim. Acta 215, 277–294. https://doi.org/10.1016/j.gca.2017.07.018.

Jaret, S.J., Hemming, S.R., Rasbury, E.T., Thompson, L.M., Glotch, T.D., Ramezani, J., Spray, J.G., 2018. Context matters – Ar–Ar results from in and around the Manicouagan Impact Structure, Canada: implications for martian meteorite chronology. Earth Planet. Sci. Lett. 501, 78–89. https://doi.org/10.1016/j.epsl.2018.08.016.

Jones, J.H., 2015. Various aspects of the petrogenesis of the Martian shergottite meteorites. Meteorit. Planet. Sci. 50, 674–690. https://doi.org/10.1111/maps.12421.

Jourdan, F., Moynier, F., Koeberl, C., Eroglu, S., 2011. ^{40}Ar/^{39}Ar age of the Lonar crater and consequence for the geochronology of planetary impacts. Geology 39, 671–674. https://doi.org/10.1130/G31888.1.

Jourdan, F., Renne, P.R., 2007. Age calibration of the Fish Canyon sanidine ^{40}Ar/^{39}Ar dating standard using primary K-Ar standards. Geochim. Cosmochim. Acta 71, 387–402. https://doi.org/10.1016/j.gca.2006.09.002.

Jourdan, F., Renne, P.R., Reimold, W.U., 2007. The problem of inherited ^{40}Ar* in dating impact glass by the ^{40}Ar/^{39}Ar method: evidence from the Tswaing impact crater (South Africa). Geochim. Cosmochim. Acta 71, 1214–1231. https://doi.org/10.1016/j.gca.2006.11.013.

Jourdan, F., Timms, N.E., Eroglu, E., Mayers, C., Frew, A., Bland, P.A., Collins, G.S., Davison, T.M., Abe, M., Yada, T., 2017. Collisional history of asteroid Itokawa. Geology 45, 819–822. https://doi.org/10.1130/G39138.1.

Jourdan, F., Verati, C., Féraud, G., 2006. Intercalibration of the HB3gr $^{40}Ar/^{39}Ar$ dating standard. Chem. Geol. 231, 177–189. https://doi.org/10.1016/j.chemgeo.2006.01.027.

Korochantseva, E.V., Trieloff, M., Buikin, A.I., Hopp, J., 2009. Shergottites Dhofar 019, SaU 005, Shergotty, and Zagami: ^{40}Ar-^{39}Ar chronology and trapped Martian atmospheric and interior argon. Meteorit. Planet. Sci. 44, 293–321.

Lapen, T.J., Righter, M., Andreasen, R., Irving, A.J., Satkoski, A.M., Beard, B.L., Kunihiko, N., Jull, A.J.T., Caffee, M.W., 2017. Two billion years of magmatism recorded from a single Mars meteorite ejection site. Sci. Adv. 3, e1600922. https://doi.org/10.1126/sciadv.1600922.

Lee, J.-Y., Marti, K., Severinghaus, J.P., Kawamura, K., Yoo, H.-S., Lee, J.B., Kim, J.S., 2006. A redetermination of the isotopic abundances of atmospheric Ar. Geochim. Cosmochim. Acta 70, 4507–4512. https://doi.org/10.1016/j.gca.2006.06.1563.

Mahaffy, P.R., Webster, C.R., Atreya, S.K., Franz, H., Wong, M., Conrad, P.G., Harpold, D., Jones, J.J., Leshin, L.A., Manning, H., Owen, T., Pepin, R.O., Squires, S., Trainer, M., MSL Science Team, 2013. Abundance and isotopic composition of gases in the Martian atmosphere from the Curiosity Rover. Science 341, 263–266. https://doi.org/10.1126/science.1237966.

McDougall, I., Wellman, P., 2011. Calibration of GA1550 biotite standard for K/Ar and $^{40}Ar/^{39}Ar$ dating. Chem. Geol. 280, 19–25. https://doi.org/10.1016/j.chemgeo.2010.10.001.

McFarlane, C.R.M., Spray, J.G., 2022. The Los Angeles martian diabase: phosphate U-Th-Pb geochronology and mantle source constraints. Geochim. Cosmochim. Acta 326, 166–179. https://doi.org/10.1016/j.gca.2022.04.006.

McKay, C.P., Toon, O.B., Kasting, J.F., 1991. Making Mars habitable. Nature 352, 489–496. https://doi.org/10.1038/352489a0.

McSween, H.Y., McLennan, S.M., 2014. Mars, Treatise on Geochemistry, 2nd edition. Elsevier, Amsterdam, pp. 251–300.

Meteoritical Bulletin Database, 2023. https://www.lpi.usra.edu/meteor/metbull.php. (Accessed 17 August 2023).

Morgan, L.E., Mark, D.F., Imlach, J., Barfod, D., Dymock, R., 2014. FCs-EK: a New Sampling of the Fish Canyon Tuff $^{40}Ar/^{39}Ar$ Neutron Flux Monitor. Special Publications, vol. 378. Geological Society, London, pp. 63–67.

Morgan, L.E., Munk, M., Davidheiser-Kroll, B., Warner, N.H., Gupta, S., Slaybaugh, R., Harkness, P., Mark, D.F., 2017. Instrumentation development for in situ $^{40}Ar/^{39}Ar$ planetary geochronology. Geostand. Geoanal. Res. 41, 381–396. https://doi.org/10.1111/ggr.12170.

Nishiizumi, K., Caffee, M.W., Masarik, J., 2000. Cosmogenic Radionuclides in Los Angeles Martian Meteorite. Metsoc. p. Abstract #5316.

Nyquist, L.E., Bogard, D.D., Shih, C.-Y., Greshake, A., Stöffler, D., Eugster, O., 2001. Ages and geologic histories of Martian meteorites. Space Sci. Rev. 96, 105–164.

Park, J., Bogard, D.D., Nyquist, L.E., Garrison, D.H., Mikouchi, T., 2013a. Ar–Ar ages and trapped Ar components in Martian shergottites RBT 04262 and LAR 06319. Geochim. Cosmochim. Acta 121, 546–570. https://doi.org/10.1016/j.gca.2013.06.045.

Park, J., Bogard, D.D., Nyquist, L.E., Herzog, G.F., 2013b. Issues in dating young rocks from another planet: Martian shergottites. In: Jourdan, F., Mark, D.F., Verati, C. (Eds.), Advances in $^{40}Ar/^{39}Ar$ Dating: from Archaeology to Planetary Sciences. The Geological Society of London, Special Publications, London, pp. 297–316.

Reiners, P.W., Carlson, R.W., Renne, P.R., Cooper, K.M., Granger, D.E., McLean, N.M., Schoene, B., 2018. Geochronology and Thermochronology. Wiley.

Renne, P.R., Balco, G., Ludwig, K.R., Mundil, R., Min, K., 2011. Response to the comment by W.H. Schwarz et al. on "Joint determination of ^{40}K decay constants and $^{40}Ar^*/^{40}K$ for the Fish Canyon sanidine standard, and improved accuracy for $^{40}Ar/^{39}Ar$ geochronology" by Paul R. Renne et al. (2010). Geochim. Cosmochim. Acta 75, 5097–5100. https://doi.org/10.1016/j.gca.2011.06.021.

Schwenzer, S.P., Greenwood, R.C., Kelley, S.P., Ott, U., Tindle, A.G., Haubold, R., Herrmann, S., Gibson, J.M., Anand, M., Hammond, S., Franchi, I.A., 2013. Quantifying noble gas contamination during terrestrial alteration in Martian meteorites from Antarctica. Meteorit. Planet. Sci. 48, 929–954. https://doi.org/10.1111/maps.12110.

Schwenzer, S.P., Herrmann, S., Ott, U., 2009. Noble gases in two shergottites and one nakhlite from Antarctica: Y000027, Y000097, and Y000593. Polar Sci. 3, 83–99. https://doi.org/10.1016/j.polar.2009.06.001.

Shampine, L.F., Reichelt, M.W., 1997. The MATLAB ODE suite. SIAM J. Sci. Comput. 18, 1–22.

Shuster, D.L., Balco, G., Cassata, W.S., Fernandes, V.A., Garrick-Bethell, I., Weiss, B.P., 2010. A record of impacts preserved in the lunar regolith. Earth Planet. Sci. Lett. 290, 155–165. https://doi.org/10.1016/j.epsl.2009.12.016.

Staddon, L.G., Darling, J.R., Schwarz, W.H., Stephen, N.R., Schuindt, S., Dunlop, J., Tait, K.T., 2021. Dating martian mafic crust; microstructurally constrained baddeleyite geochronology of enriched shergottites Northwest Africa (NWA) 7257, NWA 8679 and Zagami. Geochim. Cosmochim. Acta 315, 73–88. https://doi.org/10.1016/j.gca.2021.09.034.

Stöffler, D., Hamann, C., Metzler, K., 2018. Shock metamorphism of planetary silicate rocks and sediments: proposal for an updated classification system. Meteorit. Planet. Sci. 53, 5–49. https://doi.org/10.1111/maps.12912.

Tanaka, K.L., Robbins, S.J., Fortezzo, C.M., Skinner, J.A., Hare, T.M., 2014. The digital global geologic map of Mars: chronostratigraphic ages, topographic and crater morphologic characteristics, and updated resurfacing history. Planet. Space Sci. 95, 11–24. https://doi.org/10.1016/j.pss.2013.03.006.

Walton, E.L., Kelley, S.P., Herd, C.D.K., 2008. Isotopic and petrographic evidence for young Martian basalts. Geochim. Cosmochim. Acta 72, 5819–5837. https://doi.org/10.1016/j.gca.2008.09.005.

Walton, E.L., Sharp, T.G., Hu, J., Filiberto, J., 2014. Heterogeneous mineral assemblages in martian meteorite Tissint as a result of a recent small impact event on Mars. Geochim. Cosmochim. Acta 140, 334–348. https://doi.org/10.1016/j.gca.2014.05.023.

Weiss, B.P., Shuster, D.L., Stewart, S.T., 2002. Temperatures on Mars from $^{40}Ar/^{39}Ar$ thermochronology of ALH84001. Earth Planet. Sci. Lett. 201, 465–472.

Werner, S.C., 2009. The global Martian volcanic evolutionary history. Icarus 201, 44–68. https://doi.org/10.1016/j.icarus.2008.12.019.

Wieler, R., 2002. Cosmic-ray-produced noble gases in meteorites. Rev. Mineral. Geochem. 47, 125–170. https://doi.org/10.2138/rmg.2002.47.5.

Wiens, R.C., Becker, R.H., Pepin, R.O., 1986. The case for a martian origin of the shergottites, II. Trapped and indigenous gas components in EETA 79001 glass. Earth Planet. Sci. Lett. 77, 149–158.

Wiens, R.C., Pepin, R.O., 1988. Laboratory shock emplacement of noble gases, nitrogen, and carbon dioxide into basalt, and implications for trapped gases in shergottite EETA 79001. Geochim. Cosmochim. Acta 56, 1591–1605.

Wimpenny, J., Marks, N., Knight, K., Rolison, J.M., Borg, L., Eppich, G., Badro, J., Ryerson, F.J., Sanborn, M., Huyskens, M.H., Yin, Q., 2019. Experimental determination of Zn isotope fractionation during evaporative loss at extreme temperatures. Geochim. Cosmochim. Acta 259, 391–411. https://doi.org/10.1016/j.gca.2019.06.016.